Hindawi
International Journal of Antennas and Propagation
Volume 2022, Article ID 8363100, 11 pages
https://doi.org/10.1155/2022/8363100

Research Article

Search-Free Angle, Range, and Velocity Estimation for Monostatic FDA-MIMO

Zihang Ding, Junwei Xie, and Jiaang Ge

Air and Missile Defense College, Air Force Engineering University, Xian, China

Correspondence should be addressed to Zihang Ding; dingzihang0831@163.com

Received 9 June 2021; Revised 25 June 2022; Accepted 23 July 2022; Published 24 August 2022

Academic Editor: Stefania Bonafoni

The monostatic frequency diverse array multiple-input multiple-output (FDA-MIMO) has attracted much attention recently. However, much research is concentrated on the estimation of angle-range parameters based on the FDA-MIMO radar, and the velocity has not been considered. In this study, we propose a search-free method to estimate these parameters. To overcome the problem of the high computational complexity associated with the searching estimation algorithms, the parallel factor (PARAFAC) decomposition is introduced to estimate the space-time steering vector. Next, we can utilize the least square method to solve the angle, range, and velocity of each target. In addition, the Cramér–Rao bounds (CRBs) of angle, range, and velocity are derived. Besides, the other performance analysis consists of the root mean square error, and complexity is derived. We compare the PARAFAC decomposition algorithm with the estimation of signal parameters via the rotational invariance techniques (ESPRIT) algorithm, and our method owns a superior performance. Finally, the proposed method is verified by simulations and has the ability to achieve greater estimation accuracy than existing algorithms.

1. Introduction

Since the frequency diverse array (FDA) was first proposed in 2006, it has attracted much attention [1, 2], and more and more research studies focus on it. The beampattern of the FDA radar is related to both range and angle because of the small offset between transmit array elements [3, 4]. Thus, the FDA radar has the ability to attain additional information in range, and it can provide more flexibility in array signal processing [5, 6].

In recent years, a novel radar system called the MIMO radar attains great attention due to its special advantages [7]. Compared with the traditional phased array (PA) radar, MIMO radar brings increased degrees-of-freedoms (DoFs), and many parameter estimation algorithms have been researched in the existing literature [8, 9]. Although the MIMO radar has many obvious advantages, the beampattern of it only depends on the angle rather than both range and angle. Considering this problem, a combination of the FDA radar with MIMO was proposed in [10, 11], and it can form the beampattern which is related to range. FDA-MIMO is used in a variety of applications, including parameter estimation, deceptive jamming suppression [11, 12], target tracking [13, 14], beamspace design [15], and communication system [16].

Target multiparameter estimation, which is an important technology in array radar applications. Both angle and range can be estimated simultaneously in the FDA-MIMO radar. Multiple signal classification (MUSIC) and reduce-dimension algorithms were applied to the FDA-MIMO radar in [17, 18]. A maximum likelihood estimator to obtain angle and range parameter estimation has been proposed in [11]. The sparse reconstruction-based algorithm was implemented in angle and range estimation [19]. However, these algorithms with peak-searching need a large amount of complexity, and the complexity increases rapidly as the number of estimated parameters increases. Searching-free estimation algorithms have been used in the FDA-MIMO radar. For example, the estimation of signal parameters via rotational invariance techniques (ESPRIT) has been used to attain the range-angle parameters of target in FDA-MIMO [20–23]. In [24], the

real-valued subspace decomposition is used to estimate the angle and range.

The parallel factor (PARAFAC) decomposition was considered in the parameter estimation [25, 26] and has superior estimation accuracy and low computational complexity. PARAFAC decomposition was used to estimate the 2-D direction of arrival and frequency for an L-shaped array in [27, 28]. Because of these advantages, the algorithm has been introduced to estimate the angle and range of targets based on the FDA-MIMO radar [29].

As for the moving target localization, the information about angle, range, and velocity is crucial. However, the existing estimation methods with FDA-MIMO are only utilized in angle-range estimation, and velocity estimation has not been considered. In this study, a search-free angle-range-velocity estimation algorithm for monostatic FDA-MIMO is proposed. We utilize the PARAFAC decomposition algorithm to estimate the space-time steering vector. Once the steering vector is acquired, angle, range, and velocity can be calculated.

The remaining sections are organized as follows: Section 2 introduces the data model of FDA-MIMO. The PARAFAC algorithm is used to offer an angle-range-velocity estimation approach for the FDA-MIMO radar in Section 3. Section 4 provides a performance benchmark for the Cramér–Rao Bounds (CRBs), computational complexity, and root mean square errors (RMSE). Simulations and findings are given in Section 5. We conclude this paper in Section 6.

The PARAFAC algorithm can significantly reduce computational complexity. Results verify the effectiveness and superiority of our method. The main contributions are summarised as follows:

(1) Based on the conventional FDA-MIMO model, we introduce the Doppler frequency to the data model and expand the dimension of parameter estimation. The angle-range-velocity estimation method of the FDA-MIMO radar is proposed based on the PARAFAC decomposition algorithm.

(2) The CRBs of angle, range, and velocity are derived based on the 3-dimension parameter model of the FDA-MIMO radar.

Notation: lower-case (upper-case) bold italic characters stand for vectors (matrices). $(\cdot)^T$, $(\cdot)^H$, and $(\cdot)^\dagger$ denote the transpose, conjugate transpose, and pseudo-inverse transformation. $\otimes$ and $\circ$ are defined as the Kronecker product and the Khatri–Rao product. $\mathrm{diag}(\cdot)$ is used to build a diagonal matrix when the object is a vector or to extract diagonal elements as a vector when the object is a diagonal matrix. $\mathrm{angle}(\cdot)$ denotes the phase of the complex value.

2. Data Model

The model of monostatic FDA-MIMO is shown in Figure 1. We assume that the transmitters and receivers are from a uniform linear array with an M-element transmit array and an N-element receive array. The frequency of the m-th element can be written as

$$f_m = f_0 + (m-1)\Delta f, m = 1, 2, \ldots, M, \tag{1}$$

where f_0 denotes the carrier frequency and Δf denotes the frequency offset. Assume that the FDA-MIMO radar transmits K pulses in the CPI. The k-th transmitted pulse signal of the m-th element can be expressed as

$$\begin{aligned} g_{m,k}(t) &= \sqrt{\frac{E}{M}}\varphi_m\left(t-(k-1)T_p\right)e^{j2\pi f_m t}, \\ (k-1)T_p &< t < (k-1)T_p + T, \\ m &= 1, 2 \ldots, M, \end{aligned} \tag{2}$$

where $\varphi_m(t)$ denotes the transmitted waveform, E is the total transmit energy, and T denotes the pulse duration. According to the signal waveforms transmitted by each transmitting element being orthogonal, they are supposed to satisfy the condition [11].

$$\int_\tau \varphi_m(t)\varphi_n^*(t)e^{j2\pi(m-n)\Delta f}dt = \begin{cases} 0, m \neq n, \\ 1, m = n. \end{cases} \tag{3}$$

The signal received by the n-th element of the FDA-MIMO radar is based on P targets, and ζ_p is the complex reflection coefficient of the p-th target. The k-th pulse received signal of the n-th received element can be written as

$$r_{n,k}(t) = \sum_{p=1}^{P}\sum_{m=1}^{M}\zeta_p g_{m,k}\left(t-\tau_{m,n,k}^p\right), \tag{4}$$

$\tau_{m,n,k}^p$ denotes the propagation delay of the p-th $(p = 1, 2, \ldots, P)$ target between the m-th transmitted element and the n-th receive element at the k-th $(k = 1, 2, \ldots, K)$ pulse which is expressed as

$$\tau_{m,n,k}^p = \frac{2r_p - d_m\sin\left(\theta_p\right) - d_n\sin\left(\theta_p\right) - (k-1)v_pT_P}{c}, \tag{5}$$

where c, d denote the light speed and the element spacing, respectively. r_p, θ_p denote the range and angle of the p-th target, respectively. d_i denotes the distance between the i-th element and the reference element. T_P denotes the pulse repetition time (PRF). Under the narrowband assumption, by using (5), (4) can be updated to

$$\begin{aligned} r_{n,k}(t) &= \sqrt{\frac{E}{M}}\sum_{p=1}^{P}\sum_{m=1}^{M}\zeta_p\varphi_m \\ &\left(t-\tau_0^p\right)e^{j2\pi f_m\left(t-2r_p-d_m\sin\left(\theta_p\right)-d_n\sin\left(\theta_p\right)-(k-1)v_pT_p/c\right)}, \end{aligned} \tag{6}$$

where $\tau_0^p = 2r_p/c$ denotes the transmit time between the p-th target and the radar. Through performing matched filtering with $\varphi_m(t)e^{-j2\pi m\Delta f}$, the output corresponding to the m-th transmit element, n-th received element, the k-th pulse, and the p-th target can be expressed as [12].

$$r_{m,n,k}^p = \sqrt{\frac{E}{M}}\zeta_p e^{j2\pi\left((k-1)v_pT_P + d_m\sin\theta_p/\lambda + d_n\sin\theta_p/\lambda - \Delta f r_p/c\right)}. \tag{7}$$

Introduce the 3-dimension data model, i.e., in the case of the moving target. Assume that the p-th target has a fixed

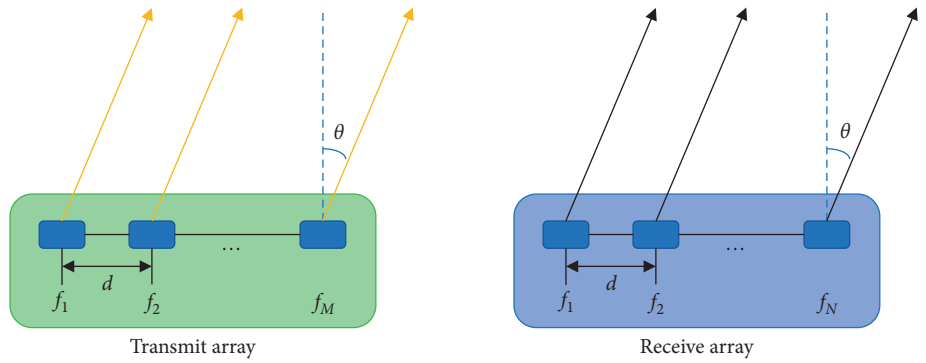

FIGURE 1: The model of the monostatic FDA-MIMO. (a) Transmit array. (b) Receive array.

velocity v_p. Rearrange the outputs of matched filters into a MNK × 1 vector, and the 3-D vector corresponding to the p-th target is written as [22].

$$\mathbf{y}_p = \zeta_p \mathbf{a}_r(\theta_p) \otimes \mathbf{c}(v_p) \otimes \mathbf{a}_t(\theta_p, r_p), \tag{8}$$

where $\mathbf{a}_r(\theta_p) \in \mathbb{C}_{N\times 1}$, $\mathbf{a}_t(\theta_p, r_p) \in \mathbb{C}_{M\times 1}$, $\mathbf{c}(v_p) \in \mathbb{C}_{K\times 1}$ denote the receive steering vector, transmit steering vector, and time steering vector, respectively. Their expressions can be written as

$$\mathbf{a}_r(\theta) = \left[1, e^{j2\pi\, d\, \sin\theta/\lambda}, \cdots, e^{j2\pi(N-1)d\, \sin\theta/\lambda}\right]^T, \tag{9}$$

$$\mathbf{a}_t(\theta, r) = \left[1, e^{j2\pi(d\, \sin\theta/\lambda - 2\Delta f r/c)}, \cdots, e^{j2\pi(M-1)(d\, \sin\theta/\lambda - 2\Delta f r/c)}\right]^T, \tag{10}$$

$$\mathbf{c}(v) = \left[1, e^{j4\pi v T_p/\lambda}, \cdots, e^{j4\pi(K-1)vT_p/\lambda}\right]^{\mathrm{T}}, \tag{11}$$

where $\lambda = c/f_0$ denotes the wavelength. From (10), the transmit vector is dependent on both the range and angle. It shows that the FDA-MIMO radar has a range of information in the transmitter. Assume that the fast time sample is L, and at the l-th sample, the total signals of P targets can be expressed as

$$\mathbf{A}_l = (\mathbf{A}_r \circ \mathbf{A}_t)\mathbf{s}(l), \tag{12}$$

with

$$\mathbf{A}_t = [\mathbf{c}(\mathrm{v}_1) \otimes \mathbf{a}_t(\theta_1, r_1), \mathbf{c}(\mathrm{v}_2) \otimes \mathbf{a}_t(\theta_2, r_2), \cdots, \mathbf{c}(\mathrm{v}_P) \otimes \mathbf{a}_t(\theta_P, r_P)], \tag{13a}$$

$$\mathbf{A}_r = [\mathbf{a}_r(\theta_1), \mathbf{a}_r(\theta_2), \cdots, \mathbf{a}_r(\theta_P)], \tag{13b}$$

where $\mathbf{s}(l)$ denotes the complex reflection coefficient of P targets at the l-th sample. Through (12), the receive signal matrix $\mathbf{Y}$ can be written as

$$\mathbf{Y} = (\mathbf{A}_r \circ \mathbf{A}_t)\mathbf{S}(t) + \mathbf{N}(t), \tag{14}$$

where $\mathbf{S}(t) = [\mathbf{s}(1), \cdots, \mathbf{s}(L)] \in \mathbb{C}_{P\times L}$, $\mathbf{N}(t) \in \mathbb{C}_{\mathrm{MNK}\times L}$ denote the signal reflection coefficient matrix and the Gaussian white noise matrix with zero mean and covariance matrix $\sigma_n \mathbf{I}_{\mathrm{MNK}}$. For convenience, define $\mathbf{c}(\mathrm{v}) \otimes \mathbf{a}_t(\theta, r) = \alpha(\theta, r, v)$.

3. Proposed Algorithm

To estimate the parameters, in general, spatial spectrum search algorithms such as the Capon and MUSIC algorithms can be utilized. However, as the dimension increases, so does the computing complexity. We presented a sequential PARAFAC algorithm in this section to estimate the angle, range, and velocity of objects, respectively.

By (12), the new received model can be written as

$$\mathbf{W}_x = \begin{bmatrix} \mathbf{Y}_1 \\ \mathbf{Y}_2 \\ \vdots \\ \mathbf{Y}_N \end{bmatrix} = \begin{bmatrix} \mathbf{A}_t D_1(\mathbf{A}_r) \\ \mathbf{A}_t D_2(\mathbf{A}_r) \\ \vdots \\ \mathbf{A}_t D_N(\mathbf{A}_r) \end{bmatrix} \mathbf{S} + \mathbf{N}_x, \tag{15}$$

where $\mathbf{N}_x = \mathbf{N}$. $D_i(\mathbf{A}_r)$ stands for a diagonal matrix constructed out of the i-th row of $\mathbf{A}_r$. Referring to the PARAFAC decomposition model in [30], the received data (15) are denoted as a three-order tensor and can be written as

$$x_{i,j,e} = \sum_{p=1}^{P} \mathbf{A}_t(i, p)\mathbf{A}_r(j, p)\mathbf{S}^T(e, p) + \mathbf{N}(i, j, e), \tag{16}$$

where $x_{i,j,k}$ denotes the (i, j, e)-th element of the three-order tensor χ, $i = 1, \ldots, MK$; $j = 1, \ldots, N$; $e = 1, \ldots, L$. $\mathbf{Y}_N$ can be viewed by slicing the three dimension data into a series of slices along the spatial direction. The model of (16) can be written as simultaneous equations along three different dimensions, and two more matrices will be expressed as

$$\mathbf{W}_y = (\mathbf{S}^T \circ \mathbf{A}_r)\mathbf{A}_t^T = \begin{bmatrix} \mathbf{A}_r D_1(\mathbf{S}^T) \\ \mathbf{A}_r D_2(\mathbf{S}_r) \\ \vdots \\ \mathbf{A}_r D_L(\mathbf{S}_r) \end{bmatrix} (\mathbf{A}_t^T) + \mathbf{N}_y, \tag{17}$$

$$\mathbf{W}_z = (\mathbf{A}_t \circ \mathbf{S}^T)\mathbf{A}_r = \begin{bmatrix} \mathbf{S}^T D_1(\mathbf{A}_t) \\ \mathbf{S}^T D_2(\mathbf{A}_t) \\ \vdots \\ \mathbf{S}^T D_{MK}(\mathbf{A}_t) \end{bmatrix} (\mathbf{A}_r^T) + \mathbf{N}_z, \tag{18}$$

where $\mathbf{W}_y$, $\mathbf{W}_z$ denote the rearrangement matrices of the three-order tensor and $\mathbf{N}_y$, $\mathbf{N}_z$ denote the rearranged noise

slices. $\mathbf{W}_y$ can be interpreted as a matrix of three-dimensional data slices arranged along the direction of the transmit array, and $\mathbf{W}_z$, $\mathbf{W}_z$ can be expressed as a matrix of three-dimensional data slices arranged along the direction of the received array. Both $\mathbf{A}_t$ and $\mathbf{A}_r$ are connected with $\mathbf{W}_x$, $\mathbf{W}_y$, $\mathbf{W}_y$, and $\mathbf{W}_z$, $\mathbf{W}_z$.

A common algorithm named trilinear alternating least square (TALS) is adopted to solve the PARAFAC effectively [26, 31]. The principle of the TALS algorithm can be expressed as follows:

Step.1: set initialization update matrix

Step.2: fitting one of $\mathbf{W}_x$, $\mathbf{W}_x$, $\mathbf{W}_y$, $\mathbf{W}_y$, $\mathbf{W}_z$, $\mathbf{W}_z$ using the LS algorithm, where the other two matrixes are obtained in the last iteration

Step.3: update the other two matrixes by step.2

Step.4: repeat Step.2 and Step.3 when the value of cost function is satisfied with the stop condition.

The detailed steps of the TALS algorithm are shown as follows:

The slice forms of the three-order tensor have been written in (15), (17), and (18). According to (15), the LS fitting of$\mathbf{W}_x$, $\mathbf{W}_x$ is

$$f_{\mathbf{x}} = \min_{\mathbf{A}_r,\mathbf{A}_t,\mathbf{S}^T} \left\| \mathbf{W}_x - (\mathbf{A}_r \circ \mathbf{A}_t)\mathbf{S} \right\|_F, \tag{19}$$

where $\|\cdot\|_F$ denotes the Frobenius norm. The LS estimate $\mathbf{S}$ can be expressed as

$$\mathbf{S} = (\mathbf{A}_r \circ \mathbf{A}_t)^{\dagger} \mathbf{W}_x, \tag{20}$$

where $\mathbf{A}_r$, $\mathbf{A}_t$ are previously obtained estimates in the last iteration. The LS fitting of $\mathbf{W}_y$ is

$$f_{\mathbf{y}} = \min_{\mathbf{A}_r,\mathbf{A}_t,\mathbf{S}^T} \left\| \mathbf{W}_y - \left(\mathbf{S}^T \circ \mathbf{A}_r\right)\mathbf{A}_t^T \right\|_F. \tag{21}$$

The update for $\mathbf{A}_t^T$ can be expressed as

$$\mathbf{A}_t^T = \left(\mathbf{S}^T \circ \mathbf{A}_r\right)^{\dagger} \mathbf{W}_y, \tag{22}$$

where $\mathbf{A}_r$, $\mathbf{S}^T$ are previously obtained estimates in the last iteration. In the same way, by (18), the LS fitting of $\mathbf{W}_z$ is

$$f_{\mathbf{z}} = \min_{\mathbf{A}_r,\mathbf{A}_t,\mathbf{S}^T} \left\| \mathbf{W}_z - \left(\mathbf{A}_t \circ \mathbf{S}^T\right)\mathbf{A}_r \right\|_F. \tag{23}$$

The update for $\mathbf{A}_t^T$, $\mathbf{A}_t^{\mathrm{T}}$ can be written as

$$\mathbf{A}_t^T = \left(\mathbf{A}_t \circ \mathbf{S}^T\right)^{\dagger} \mathbf{W}_z, \tag{24}$$

where $\mathbf{A}_t$, $\mathbf{S}^T$ are previously obtained estimates in the last iteration, respectively.

According to the (20), (22), and (24), $\mathbf{S}^T$, $\mathbf{S}^{\mathrm{T}}$, $\mathbf{A}_t$, $\mathbf{A}_t$, and $\mathbf{A}_r$ are calculated with the LS algorithm. The iteration can repeat until the method convergence or reaching the maximum number of iterations.

The received and transmitted steering vectors of the p-th target are estimated as $\overline{\mathbf{a}}_r(\theta_p)$, $\overline{\alpha}(\theta_p, r_p, v_p)$. The angle can be estimated first. The phase of the normalization version of $\overline{\mathbf{a}}_r(\theta_p)$ can be obtained.

$$\overline{\mathbf{g}}_{rp} = -\text{angle}\left(\frac{\overline{\mathbf{a}}_r(\theta)}{\overline{\mathbf{a}}_r(\theta)[1]}\right), \tag{25}$$

where $\overline{\mathbf{a}}_r(\theta)[1]$ denotes the first element in the string vector $\overline{\mathbf{a}}_r(\theta)$. To obtain the angle of targets, we construct a matrix as follows:

$$\mathbf{U}_1 = \begin{bmatrix} 1 & 1 & \cdots & 1 \\ 0 & \dfrac{2\pi\, d}{\lambda} & \cdots & \dfrac{2(N-1)\pi\, d}{\lambda} \end{bmatrix}^T, \tag{26}$$

$$\mathbf{u}_p = \begin{bmatrix} u_{p1} & u_{p2} \end{bmatrix}^T. \tag{27}$$

The solution to LS fitting for $\mathbf{u}_p$ is known as $\mathbf{u}_p = \mathbf{U}_1^{\dagger}\overline{\mathbf{g}}_{rp}$. Then, the angle of the p-th target is expressed as

$$\overline{\theta}_p = \arcsin\left(u_{p2}\right) \cdot \frac{180}{\pi}. \tag{28}$$

Secondly, the range of the p-th target is estimated. Obtaining the phase of the normalization version of $\overline{\alpha}(\theta_p, r_p, v_p)[1\colon M]$

$$\overline{\mathbf{g}}_{tp} = -\text{angle}\left(\frac{\overline{\boldsymbol{\alpha}}\left(\theta_p, r_p, v_p\right)[1\colon M]}{\overline{\boldsymbol{\alpha}}\left(\theta_p, r_p, v_p\right)[1]}\right), \tag{29}$$

where $\overline{\alpha}(\theta_p, r_p, v_p)[1\colon M]$ presents a vector with the first element to the m-th element in $\overline{\alpha}(\theta_p, r_p, v_p)$. Similarly, a matrix will be constructed as follows:

$$\mathbf{U}_2 = \begin{bmatrix} 1 & 1 & \cdots & 1 \\ 0 & 2\pi & \cdots & 2\pi(M-1) \end{bmatrix}^T, \tag{30}$$

$$\mathbf{q}_p = \begin{bmatrix} q_{p1} & q_{p2} \end{bmatrix}^T. \tag{31}$$

The solution to LS fitting for $\mathbf{q}_p$ is known as $\mathbf{q}_p = \mathbf{U}_2^{\dagger}\overline{\mathbf{g}}_{tp}$. The range of the p-th target can be expressed as

$$r_p = \frac{\left(\left(d\, \sin\left(\theta_p\right)/\lambda\right) - q_{p2}\right)c}{\Delta f}. \tag{32}$$

To avoid the unambiguity phase of the range parameter, the constrained range can be given by $r_{\max} < c/\Delta f$.

Here, θ_p can be estimated by (28). Finally, the velocity of the p-th target is estimated. The phase of the normalization version of $\overline{\alpha}(\theta_p, r_p, v_p)[1, M+1, \cdots, (K-1)M+1]$ is attained.

$$\overline{\mathbf{g}}_{vp} = -\text{angle}\left(\frac{\overline{\boldsymbol{\alpha}}\left(\theta_p, r_p, v_p\right)[1, M+1, \cdots, (K-1)M+1]}{\overline{\boldsymbol{\alpha}}\left(\theta_p, r_p, v_p\right)[1]}\right), \tag{33}$$

where $\overline{\alpha}(\theta_p, r_p, v_p)[1, M+1, \cdots, (K-1)M+1]$ denotes a vector with the 1th, $(M+1)$-th, . . ., $(M(K-1)+1)$-th element in $\overline{\alpha}(\theta_p, r_p, v_p)$. Similarly, a matrix will be constructed as follows:

$$\mathbf{U}_3 = \begin{bmatrix} 1 & 1 & \cdots & 1 \\ 0 & 2\pi & \cdots & 2\pi(K-1) \end{bmatrix}^T, \tag{34}$$

$$\mathbf{h}_p = \begin{bmatrix} h_{p1} & h_{p2} \end{bmatrix}^T. \tag{35}$$

The solution to LS fitting for $\mathbf{h}_p$ can be known as $\mathbf{h}_p = \mathbf{U}_3^{\dagger}\overline{\mathbf{g}}_{vp}$, and the velocity can be expressed as

$$v_p = \frac{h_{p2}\lambda}{(2T_R)}. \tag{36}$$

4. Performance Analysis

4.1. Cramér–Rao Bound. We will derive the formula of the Cramér–Rao bounds (CRBs) in this subsection for angle, range, and velocity estimation. Assume that there is just one target and that the reflection coefficient is constant when deriving the CRBs.

By (12), the received signal can be written as

$$\mathbf{y} = \mathbf{a}_r(\theta) \otimes \boldsymbol{\alpha}(\theta, r, v)\mathbf{S}+\mathbf{N} = \mathbf{b}(\theta, r, v)\mathbf{S}+\mathbf{N}. \tag{37}$$

The unknown parameter vector is

$$\xi = [\theta, r, v]^T. \tag{38}$$

The corresponding Fisher information matrix (FIM) can be derived as

$$\mathbf{F} = 2L\mathrm{Re}\left\{\left(\frac{\partial \mathbf{b}(\theta, r, v)}{\partial \boldsymbol{\xi}^T}\right)^H \mathbf{R}_n^{-1}\left(\frac{\partial \mathbf{b}(\theta, r, v)}{\partial \boldsymbol{\xi}^T}\right)\right\}, \tag{39}$$

where $\mathbf{R}_n = \sigma^2\mathbf{I}_{\mathrm{MNK}\times\mathrm{MNK}}$ denotes the noise covariance matrix and σ^2 and L denote the noise power and the number of snapshots, respectively. The partial derivative can be written as

$$\frac{\partial \mathbf{b}(\theta, r, v)}{\partial \boldsymbol{\xi}^T} = \left[\frac{\partial \mathbf{b}(\theta, r, v)}{\partial \theta}, \frac{\partial \mathbf{b}(\theta, r, v)}{\partial r}, \frac{\partial \mathbf{b}(\theta, r, v)}{\partial v}\right], \tag{40}$$

whose terms can be given by

$$\frac{\partial \mathbf{b}(\theta, r, v)}{\partial \theta} = \frac{\partial \mathbf{a}_r(\theta)}{\partial \theta} \otimes \left(\mathbf{c}(v) \otimes \frac{\partial \mathbf{a}_t(\theta, r)}{\partial \theta}\right), \tag{41a}$$

$$\frac{\partial \mathbf{b}(\theta, r, v)}{\partial r} = \mathbf{a}_r(\theta) \otimes \left(\mathbf{c}(v) \otimes \frac{\partial \mathbf{a}_t(\theta, r)}{\partial r}\right), \tag{41b}$$

$$\frac{\partial \mathbf{b}(\theta, r, v)}{\partial v} = \mathbf{a}_r(\theta) \otimes \left(\frac{\partial \mathbf{c}(v)}{\partial v} \otimes \mathbf{a}_t(\theta, r)\right), \tag{41c}$$

with

$$\frac{\partial \mathbf{a}_r(\theta)}{\partial \theta} = \frac{j2\pi d \cos\ \theta}{\lambda \boldsymbol{\Lambda}_N \mathbf{a}_r(\theta)}, \tag{42a}$$

$$\frac{\partial \mathbf{a}_t(\theta, r)}{\partial \theta} = \frac{j2\pi d \cos\ \theta}{\lambda \boldsymbol{\Lambda}_M \mathbf{a}_t(\theta, r)}, \tag{42b}$$

$$\frac{\partial \mathbf{a}_t(\theta, r)}{\partial r} = -\frac{j2\pi\Delta f}{c\boldsymbol{\Lambda}_M \mathbf{a}_t(\theta, r)}, \tag{42c}$$

$$\frac{\partial \mathbf{c}(v)}{\partial v} = \frac{4\pi T_p}{\lambda \boldsymbol{\Lambda}_K \mathbf{c}(v)}, \tag{42d}$$

where $\Lambda_P = \mathrm{diag}(0, 1, \ldots, P-1)$. The inverse of the FIM can be expressed as

$$\mathbb{Q} = \mathbf{F}^{-1}. \tag{43}$$

The diagonal elements of $\mathbb{Q}$ are the CRBs for angle (θ), range (r), and velocity (v) estimations, respectively.

4.2. Complexity Analysis. The main aim is to reduce the complexity of the multiple parameter estimation with no searching estimation algorithm. There is large complexity when the spectral peak searching algorithms are used. The 3D-MUSIC requires $O\{n_\theta n_r n_v[\mathrm{MNK}(\mathrm{MNK}-P)+(\mathrm{MNK}-P)]+2(\mathrm{MNK})^2L+(\mathrm{MNK})^3\}$. The ESPRIT algorithm requires $O\{N^2M^2K^2L+(\mathrm{MNK})^3+2MK(N-1)P^2+2NK(M-1)P^2+3P^3+2NM(K-1)P^2\}$.

The OMP algorithm requires $O\{\mathrm{NMK}n_\theta n_r n_v+\mathrm{NMK}P^2+\mathrm{NMK}P+P^3\}$. The computational complexity of the TALS algorithm for PARAFAC decomposition is $O\{l[3P^3+3\mathrm{MNKL}P+(2\mathrm{P}^2+P)(\mathrm{MKL}+NL+\mathrm{MKN})]\}$, where l is the number of iterations. The computational complexity in Equations (26)–(28), Equations (30)–(32), and Equations (30)–(32) is $O\{2PM+2PN+2PK\}$.

4.3. Root Mean Square Error. To assess the estimation (angle, range, and velocity) performance, the root mean square of error (RMSE) is adopted. The RMSE can be expressed as

$$\mathrm{RMSE}_\theta = \frac{1}{P}\sum_{p=1}^{P}\sqrt{\frac{1}{B}\sum_{b=1}^{B}\left(\overline{\theta}_{p,b}-\theta_{p,b}\right)^2}, \tag{44a}$$

$$\mathrm{RMSE}_r = \frac{1}{P}\sum_{p=1}^{P}\sqrt{\frac{1}{B}\sum_{b=1}^{B}\left(\overline{r}_{p,b}-r_{p,b}\right)^2}, \tag{44b}$$

$$\mathrm{RMSE}_v = \frac{1}{P}\sum_{p=1}^{P}\sqrt{\frac{1}{B}\sum_{b=1}^{B}\left(\overline{v}_{p,b}-v_{p,b}\right)^2}, \tag{44c}$$

where B denotes the number of the Monte Carlo trials.

4.4. The Selection of Frequency Offset. According to radar theories, the maximum unambiguous range can be expressed as

$$r_{\mathrm{up}} = \frac{c}{(2f_{\mathrm{PRF}})}, \tag{45}$$

where f_{PRF} denotes the PRF of the FDA-MIMO radar.

In addition, to avoid the multiple solution of estimated range, the frequency increment Δf should be satisfied as

$$\frac{c}{2\Delta f} > r_{\max}. \tag{46}$$

Table 1: The simulation parameters of the FDA-MIMO radar.

Parameters	Values
Transmit elements	9
Receive elements	8
Element spacing	Half-waveform
Number of snapshots	256
Number of coherent pulses	7
Carrier frequency	6×10^9Hz
Frequency increment	3 KHz

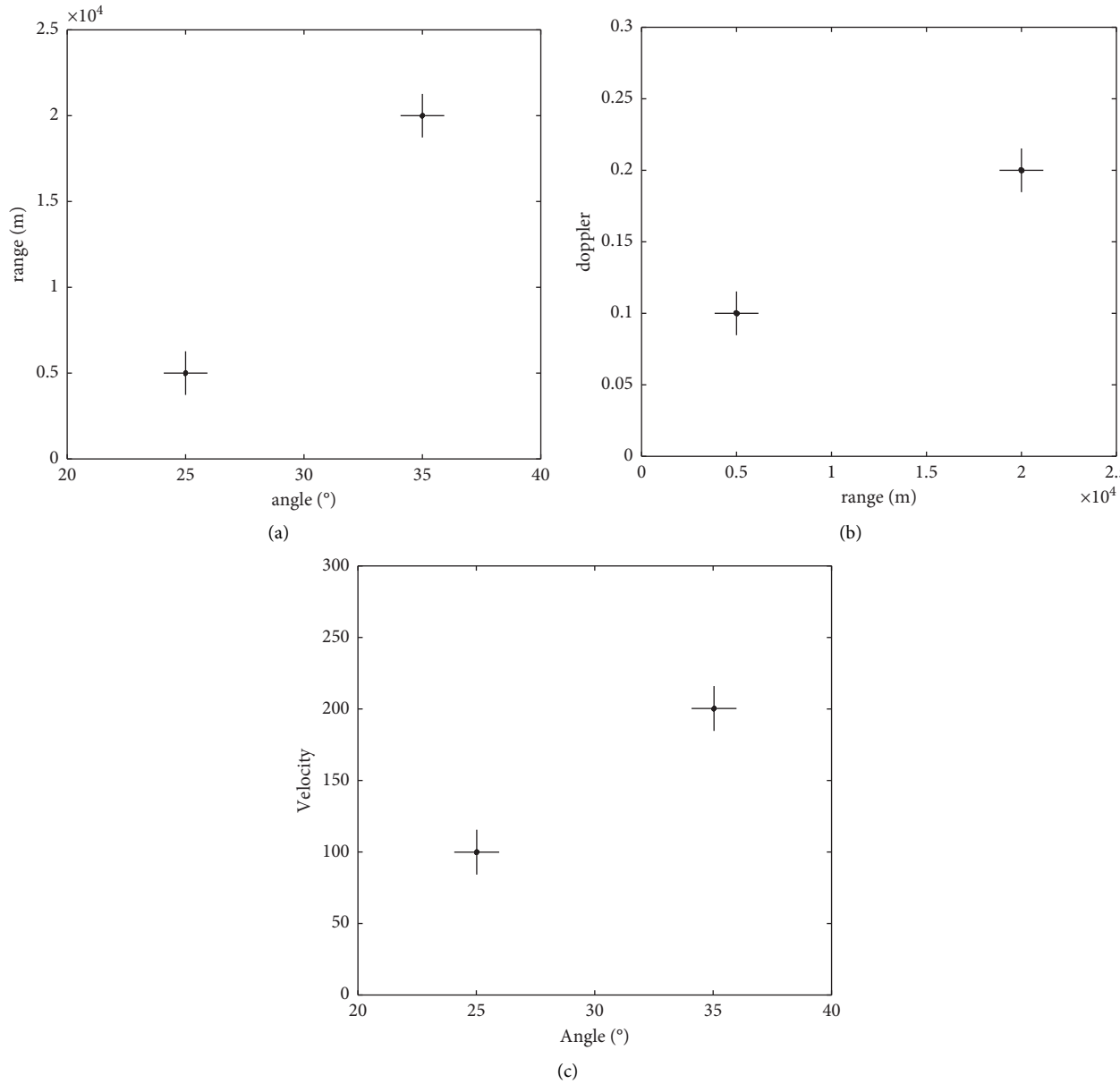

Figure 2: Scatter estimation results of the proposed algorithm. (a) The angle and range estimation result, (b) the range and velocity estimation result, and (c) the angle and velocity estimation result.

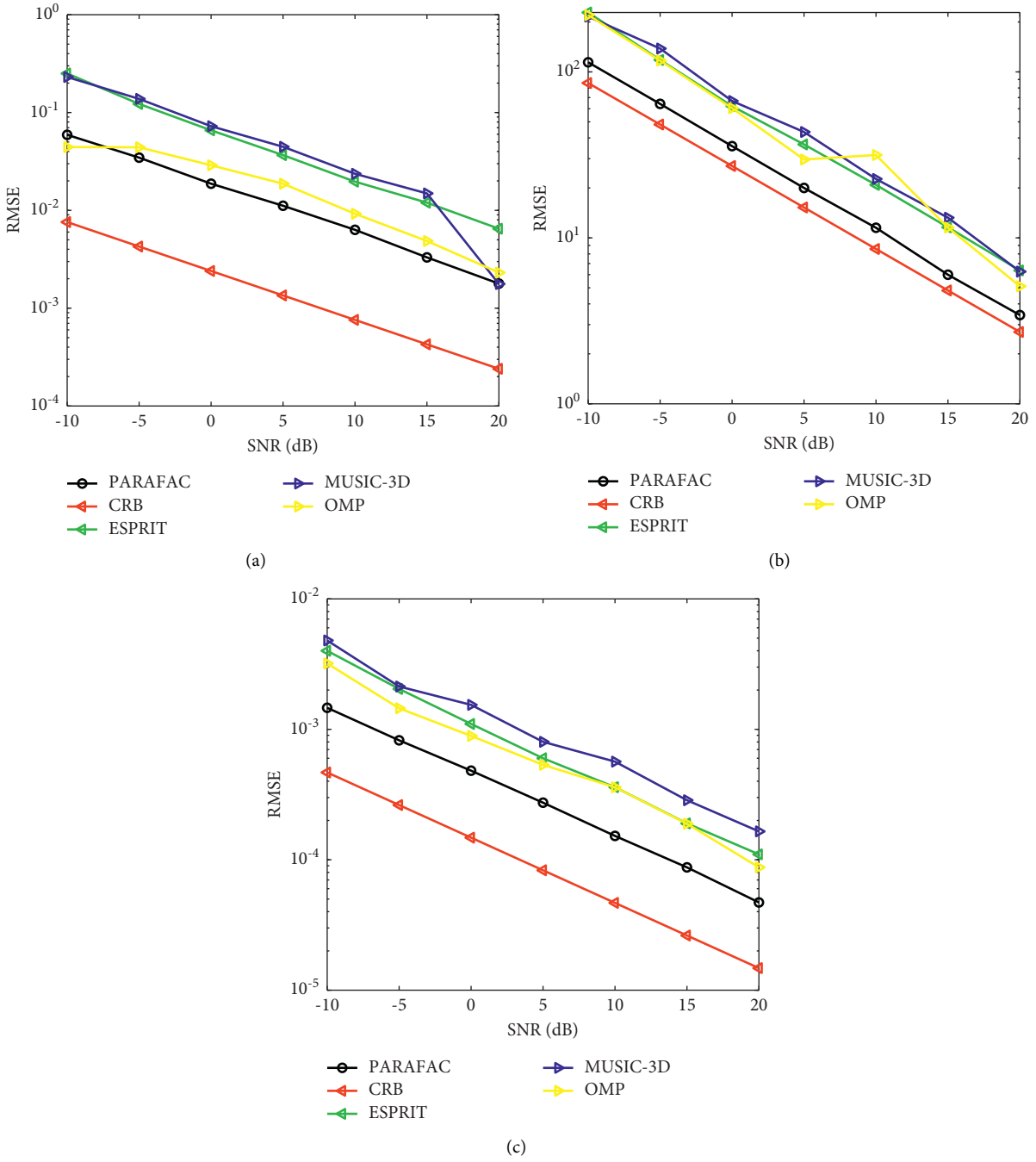

Figure 3: RMSEs and CRB versus SNR for parameter estimation (a) the angle, (b) the range, and (c) the velocity.

The maximum unambiguous velocity can be expressed as

$$v_{\text{up}} = \frac{\lambda f_{\text{PRF}}}{2}. \tag{47}$$

We proposed a selection criterion [11] of frequency offset, and it can be provided as

$$\Delta f = \max_q \{(q+v) f_{\text{PRF}}\}, q \in \mathbb{N},$$
$$\text{s.t} \begin{cases} v = \dfrac{1}{N_a} \\ \Delta f \le \dfrac{B}{2N_a} \end{cases}, \tag{48}$$

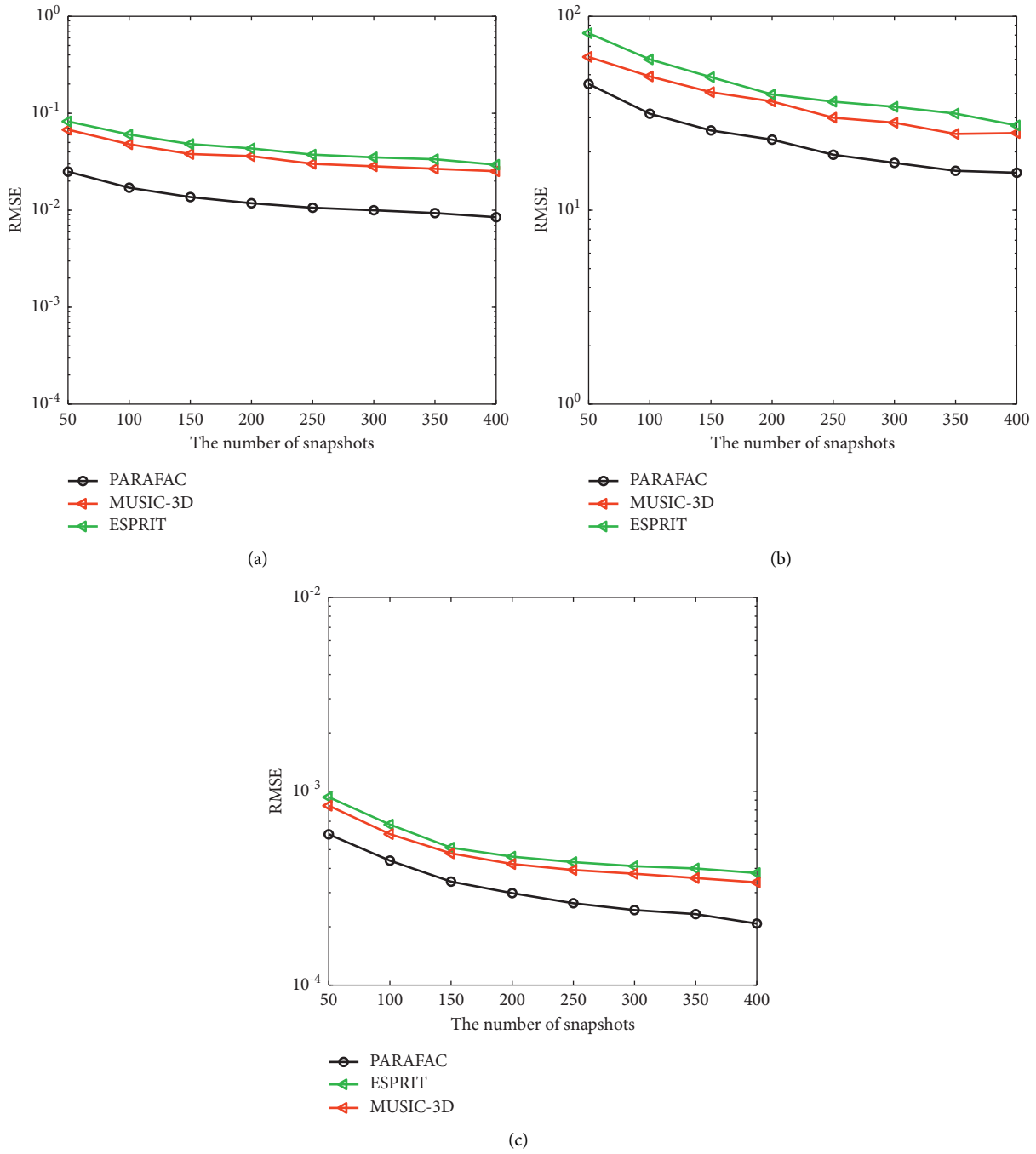

Figure 4: The RMSE versus the number of snapshots. (a) The angle, (b) the range, and (c) the velocity.

B denotes the signal bandwidth, $N_a = \text{int}(M - 1/2)$, where $\text{int}(x)$ indicates the smallest integer greater than or equal to x.

5. Simulation Result

$B = 500$ Monte Carlo trials are used to evaluate the accuracy of the proposed method. The simulation parameters of a monostatic FDA-MIMO radar are shown in Table 1.

We assume that there are $P = 2$ uncorrelated sources located at $(\theta_1, r_1) = (25^\circ, 5\text{km})$, $(\theta_2, r_2) = (35^\circ, 20\text{km})$. The normalized Doppler shifts are $f_{d1} = 0.1$, $f_{d2} = 0.2$, and the corresponding velocities are $v_1 = 100m/s$ and $v_2 = 200m/s$, $v_2 = 200\text{m/s}$.

Set the value of the SNR as 5 dB. The proposed method's scatter estimate results are shown in Figure 2. The proposed method is capable of accurately estimating angles, ranges, and velocities. The estimation results are close to the actual scenario.

Figure 3 shows the RMSE_θ, RMSE_r, RMSE_v comparisons of different methods such as MUSIC, ESPRIT, and Orthogonal Matching Pursuit (OMP) algorithms versus SNR. We can find that the proposed method attains a superior

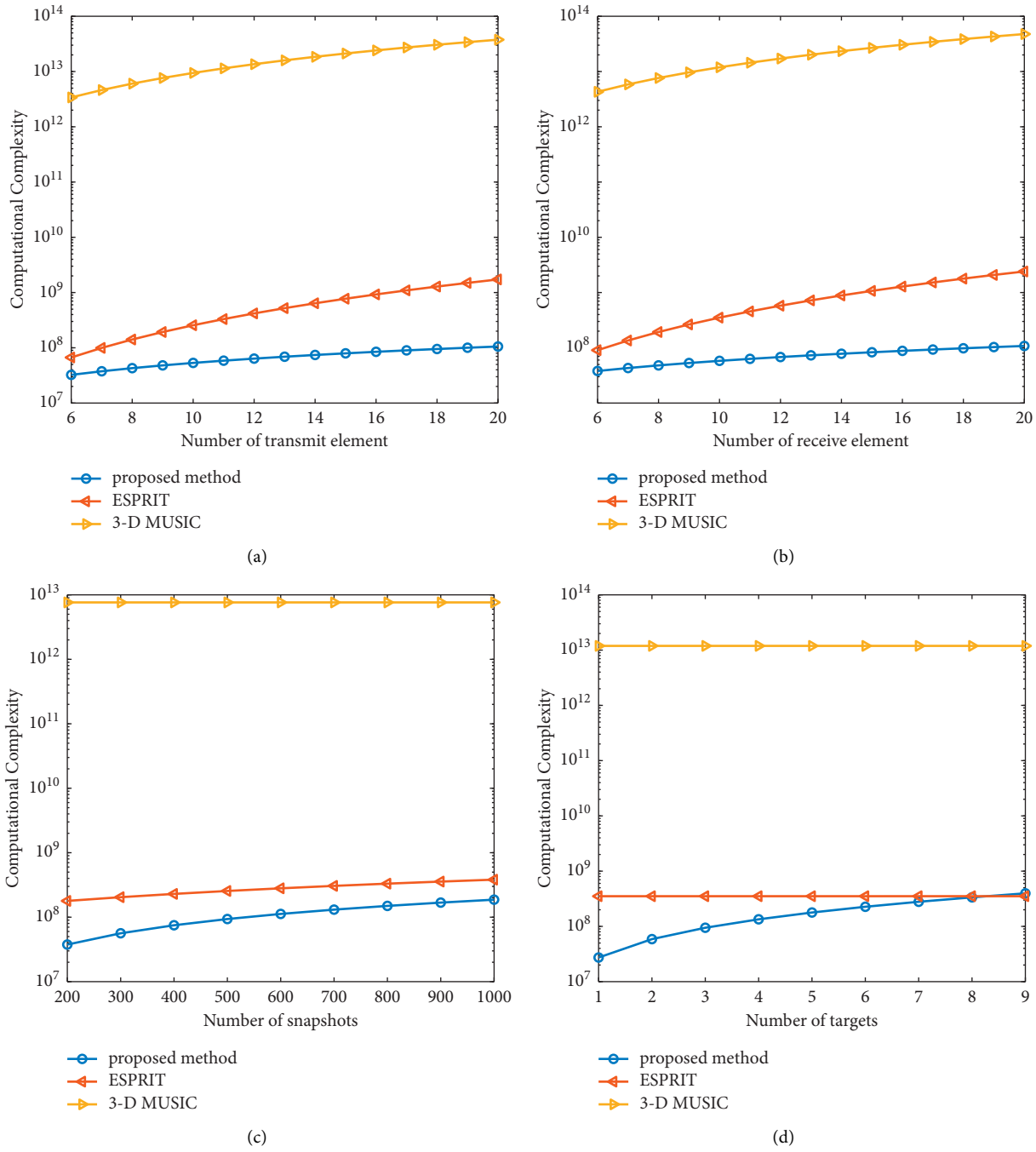

FIGURE 5: The computational complexity among different algorithms. (a) Complexity versus the number of transmit elements, (b) complexity versus the number of receive elements, (c) complexity versus the number of snapshots, and (d) complexity versus the number of targets.

angle, range, and velocity estimation performance to other algorithms. In addition, the range estimation accuracy is close to the CRB by the proposed method.

To evaluate the estimation performance of different number of snapshots, we calculate the RMSE of different estimation algorithms in different number of snapshots with a fixed SNR = 5, and the result is shown in Figure 4. In Figures 4(a)–4(c), we can find that the RMSEs of the angle, range, and velocity are slightly decreasing versus the increasing number of snapshots.

The computational complexity is compared among PARAFAC, ESPRIT, and 3D-MUSIC in Figure 5. The simulation parameters are set as follows: $P = 2$, $l = 30$, the number of searching grids corresponding to the angle, range, and velocity is $n_\theta = 300, n_r = 1000$, and $n_v = 100$, respectively. According to the results, the proposed algorithm and the ESPRIT algorithm have much lower complexity than the 3D-MUSIC. Figures 5(a) and 5(b) show the complexity versus the number of transmit and receive elements, and we can find that the complexities of 3D-MUSIC and ESPRIT are rising faster

than PARAFAC. In Figure 5(c), the complexity versus the number of snapshots has no significant change. Figure 5(d) shows the complexity versus the number of targets, and we can find that the complexity of the proposed algorithm increases versus the number of targets, and the number of targets has a small impact on 3D-MUSIC and ESPRIT.

6. Conclusion

The angle and range estimation based on the FDA-MIMO radar has attracted much attention. However, the velocity of the moving target cannot be estimated directly. In this paper, the information in the angle-range-velocity domains is combined. We concentrate on the angle, range, and velocity estimation with search-free algorithms for monostatic FDA-MIMO. The PARAFAC algorithm is used to estimate the steering vectors, and we can calculate the angle, range, and velocity of the targets from the estimated steering vectors. Because of the velocity, the dimension of the steering vector is greatly improved, which leads to an increase in computational complexity. Both theoretical analysis and simulations indicate that the PARAFAC algorithm has much lower complexity than the 3D-MUSIC algorithm. The proposed algorithm can attain a higher estimation accuracy than ESPRIT, MUSIC, and OMP. [32–36].

Data Availability

No data were used to support this study.

Conflicts of Interest

The authors declare that they have no conflicts of interest.

Acknowledgments

National Nature Science Foundation of China under Grants 62001506.

References

[1] P. Antonik, M. C. Wicks, H. D. Griffiths, and C. J. Baker, "Range dependent beamforming using element level waveform diversity," in *Proceedings of the Int. Waveform Diversity and Design Conf*, pp. 22–27, Lihue, HI, USA, January 2006.

[2] P. Antonik, M. C. Wicks, H. D. Griffiths, and C. J. Baker, "Multi-mission multi-mode waveform diversity," in *Proceedings of the IEEE Conf. on Radar*, pp. 580–582, Verona, NY, USA, April 2006.

[3] M. Secmen, S. Demir, A. Hizal, and T. Eker, "Frequency Diverse Array Antenna with Periodic Time Modulated Pattern in Range and Angle," in *Proceedings of the IEEE Radar Conf*, pp. 427–430, Boston, MA, USA, April 2007.

[4] J. J. Huang, K. F. Tong, and C. J. Baker, "Frequency diverse array: simulation and design," in *Proceedings of the IEEE Radar Conf*, pp. 1–4, Pasadena, CA, USA, May 2009.

[5] K. Gao, W. Q. Wang, H. Chen, and J. Y. Cai, "Transmit beamspace design for multi-carrier frequency diverse array sensor," *IEEE Sensors Journal*, vol. 16, no. 14, pp. 5709–5714, 2016.

[6] W. Q. Wang, "Frequency diverse array antenna: new opportunities," *IEEE Antennas and Propagation Magazine*, vol. 57, no. 2, pp. 145–152, 2015.

[7] M. Akcakaya and A. Nehorai, "MIMO radar sensitivity analysis for target detection," *IEEE Transactions on Signal Processing*, vol. 59, pp. 3241–3250, 2011.

[8] X. P. Wang, M. X. Huang, and L. T. Wan, "Joint 2D-DOD and 2D-DOA estimation for coprime EMVS–MIMO radar," *Circuits, Systems, and Signal Processing*, vol. 40, no. 6, pp. 2950–2966, 2021.

[9] L. T. Wan, K. H. Liu, Y. C. Liang, and T. Zhu, "DOA and polarization estimation for non-circular signals in 3-D millimeter wave polarized massive MIMO systems," *IEEE Transactions on Wireless Communications*, vol. 20, no. 5, pp. 3152–3167, 2021.

[10] P. F. Sammartino, C. J. Baker, and H. D. Griffiths, "Frequency diverse MIMO techniques for radar," *IEEE Transactions on Aerospace and Electronic Systems*, vol. 49, no. 1, pp. 201–222, 2013.

[11] J. W. Xu, G. S. Liao, S. Q. Zhu, L. Huang, and H. C. So, "Joint range and angle estimation using MIMO radar with frequency diverse array," *IEEE Transactions on Signal Processing*, vol. 63, no. 13, pp. 3396–3410, 2015.

[12] Z. H. Ding, J. W. Xie, B. Wang, and H. W. Zhang, "Robust adaptive null broadening method based on FDA-MIMO radar," *IEEE Access*, vol. 8, pp. 177976–177983, 2020.

[13] A. Basit, W.-Q. Wang, S. Y. Nusenu, and Z. Zheng, "Cognitive FDA-MIMO with channel uncertainty information for target tracking," *IEEE Transactions on Cognitive Communications and Networking*, vol. 5, no. 4, pp. 963–975, 2019.

[14] A. Basit, W.-Q. Wang, and S. Y. Nusenu, "Adaptive transmit array sidelobe control using FDA-MIMO for tracking in joint radar-communications," *Digital Signal Processing*, vol. 97, pp. 1–13, 2020.

[15] A. Basit, W.-Q. Wang, S. Wali, and S. Yaw Nusenu, "Transmit beamspace design for FDA–MIMO radar with alternating direction method of multipliers," *Signal Processing*, vol. 180, Article ID 107832, 2021.

[16] S. Y. Nusenu, W.-Q. Wang, and A. Basit, "Time-modulated FD-MIMO array for integrated radar and communication systems," *IEEE Antennas and Wireless Propagation Letters*, vol. 17, no. 6, pp. 1015–1019, 2018.

[17] J. Xiong, W. Q. Wang, and K. D. Gao, "FDA-MIMO radar range-angle estimation: CRLB, MSE, and resolution analysis," *IEEE Transactions on Aerospace and Electronic Systems*, vol. 54, no. 1, pp. 284–294, 2018.

[18] M. Feng, Z. Cui, Y. Yang, and Q. Shu, "A reduced-dimension MUSIC algorithm for monostatic FDA-MIMO radar," *IEEE Communications Letters*, vol. 25, no. 4, pp. 1279–1282, 2021.

[19] H. Chen and H. Shao, "Sparse reconstruction based target localization with frequency diverse array MIMO radar," in *Proceedings of the IEEE China Summit and International Conf*, pp. 1–7, Chengdu, China, July 2015.

[20] Y. Yan, J. Cai, and W. Q. Wang, "Two-stage ESPRIT for unambiguous angle and range estimation in FDA-MIMO radar," *Digital Signal Processing*, vol. 92, pp. 151–165, 2019.

[21] F. L. Liu, X. P. Wang, M. X. Huang, L. Wan, H. Wang, and B. Zhang, "A novel unitary ESPRIT algorithm for monostatic FDA-MIMO radar," *Sensors*, vol. 20, no. 3, pp. 1–17, 2020.

[22] B. B. Li, W. Bai, and G. Zheng, "Successive ESPRIT algorithm for joint DOA-range-polarization estimation with polarization sensitive FDA-MIMO radar," *IEEE Access*, vol. 6, pp. 36376–36382, 2018.

[23] Y. W. Song, G. M. Zheng, and G. P. Hu, "A combined ESPRIT-MUSIC method for FDA-MIMO radar with extended range ambiguity using staggered frequency increment," *International Journal of Antennas and Propagation*, vol. 2019, pp. 1–7, Article ID 3056074, 2019.

[24] F. L. Liu, X. P. Wang, M. X. Huang, and L. T. Wan, "Joint angle and range estimation for bistatic FDA-MIMO radar via real-valued subspace decomposition," *Signal Processing*, vol. 185, Article ID 108065, 2021.

[25] N. D. Sidiropoulos, R. Bro, and G. B. Giannakis, "Parallel factor analysis in sensor array processing," *IEEE Transactions on Signal Processing*, vol. 48, no. 8, pp. 2377–2388, 2000.

[26] X. Zhang, Z. Xu, L. Xu, and D. Xu, "Trilinear decomposition-based transmit angle and receive angle estimation for multiple-input multipleoutput radar," *IET Radar, Sonar & Navigation*, vol. 5, no. 6, pp. 626–631, 2011.

[27] R. Wu, L. Xu, Z. Zhang, and Y. Dong, "Joint 2-D DOA and Doppler estimation for L-shaped array via dual PARAFAC with triple matching implementation," *IEEE Access*, vol. 7, pp. 51749–51758, 2019.

[28] L. Xu, R. Wu, X. Zhang, and Z. Shi, "Joint two-dimensional DOA and frequency estimation for L-shaped array via compressed sensing PARAFAC method," *IEEE Access*, vol. 6, pp. 37204–37213, 2018.

[29] C. Cui, J. Xu, R. Gui, W. Q. Wang, and W. Wu, "Search-free DOD, DOA and range estimation for bistatic FDA-MIMO radar," *IEEE Access*, vol. 6, pp. 15431–15445, 2018.

[30] F. Q. Wen, X. D. Xiong, and Z. J. Zhang, "Angle and mutual coupling estimation in bistatic MIMO radar based on PARAFAC decomposition," *Digital Signal Processing*, vol. 65, pp. 1–10, 2017.

[31] J. F. Li and M. Zhou, "Improved trilinear decomposition-based method for angle estimation in multiple-input multiple-output radar," *IET Radar, Sonar & Navigation*, vol. 7, no. 9, pp. 1019–1026, 2013.

[32] W. T. Li, C. Cui, X. T. Ye, X. W. Shi, and H. C. So, "Quasi-time-invariant 3-D focusing beampattern synthesis for conformal frequency diverse array," *IEEE Transactions on Antennas and Propagation*, vol. 68, no. 4, pp. 2684–2697, 2020.

[33] C. Wen, C. Z. Ma, J. Y. Peng, and J. X. Wu, "Bistatic FDA-MIMO radar space-time adaptive processing," *Signal Processing*, vol. 163, pp. 201–212, 2019.

[34] W. Q. Wang, "Overview of frequency diverse array in radar and navigation applications," *IET Radar, Sonar & Navigation*, vol. 10, no. 6, pp. 1001–1012, 2016.

[35] J. W. Xu, G. S. Liao, S. Q. Zhu, and H. C. So, "Deceptive jamming suppression with frequency diverse MIMO radar," *Signal Processing*, vol. 113, pp. 9–17, 2015.

[36] W. Q. Wang, H. Z. Shao, and J. Y. Cai, "Range-angle-dependent beamforming by frequency diverse array antenna," *International Journal of Antennas and Propagation*, vol. 2012, pp. 1–10, Article ID 760489, 2012.